Available online at www.sciencedirect.com
ScienceDirect
Journal of Molecular Catalysis A: Chemical 283 (2008) 43–51
JOURNAL OF MOLECULAR CATALYSIS A: CHEMICAL
www.elsevier.com/locate/molcata

The CO adsorption on a Fe_2O_3–$Ce_{0.5}Zr_{0.5}O_2$ catalyst studied by TPD, isotope exchange and FTIR spectroscopy

Vladimir Galvita [a], Liisa K. Rihko-Struckmann [b,*], Kai Sundmacher [a,b]

[a] *Otto-von-Guericke University Magdeburg, Process Systems Engineering, Universitätsplatz 2, D-39106 Magdeburg, Germany*
[b] *Max Planck Institute for Dynamics of Complex Technical Systems, Sandtorstrasse 1, D-39106 Magdeburg, Germany*

Received 11 September 2007; received in revised form 2 November 2007; accepted 5 November 2007
Available online 26 November 2007

Abstract

The interaction of carbon monoxide with Fe_2O_3–$Ce_{0.5}Zr_{0.5}O_2$ was investigated by the adsorption investigation under isothermal CO/H_2 exposure and temperature-programmed desorption (TPD), as well as by in-situ diffuse-reflectance infrared Fourier transform spectroscopy (DRIFTS), in order to understand the carbon monoxide formation during the cyclic water gas shift reaction. When the Fe_2O_3–$Ce_{0.5}Zr_{0.5}O_2$ catalyst was exposed to a mixture of CO and H_2, the majority of the surface species depicted by the DRIFT analysis were associated with carbonates. The carbonates were essentially stable in a He atmosphere at temperatures ranging from 60 to 450 °C. An increase in the temperature leads to the conversion of the carbonates, where the oxygen comes from the catalyst lattice. Investigations carried out using a H_2O/He mixture showed that carbon oxides were produced during the interconversion of carbonate species on the catalyst surface with steam. The main gas component produced during the TPD of an Fe_2O_3–$Ce_{0.5}Zr_{0.5}O_2$ catalyst in the temperature interval of 60–500 °C was carbon dioxide. The amount of carbon oxides produced decreased at elevated temperatures. The steady-state isotopic $C^{18}O$ experiments revealed that the Boudouard reaction occurred at temperatures higher than 350 °C. The carbon deposits which were formed on the catalyst surface during the reduction step through the Boudouard reaction led to CO formation during the successive re-oxidation step.

Keywords: Cyclic water gas shift reaction; WGS; Fe_2O_3–$Ce_{0.5}Zr_{0.5}O_2$; DRIFTS; TPD; Isotope exchange

1. Introduction

During the last two decades, the direct utilisation of hydrogen as clean fuel or as feed for producing other fuels and commodities has become a percipient alternative to the utilisation of non-regenerative fossil energy [1]. Hydrogen is expected to play a major role as a carbon-free energy carrier in the future. Although it can be burnt without CO_2 emissions also in traditional internal combustion engines, the utilisation of hydrogen in fuel cells is especially advantageous, as fuel cells work at a high efficiency and without emitting any toxic emissions. Today, on an industrial scale, H_2 is produced from hydrocarbon fuels or alcohols by reforming processes. The product streams of a reforming process typically contain mixtures of H_2, CO, CO_2 and H_2O. However, high-purity, CO-free hydrogen is needed for the operation of a low-temperature polymer electrolyte membrane fuel cell (PEM-FC) [1]. The CO level in the hydrogen gas mixture has to be reduced below 20 ppm in order to avoid severe poisoning of the catalyst at the fuel cell electrodes [1–4]. CO-free H_2 can be produced by a multi-step purification process that includes two water-gas shift reactors coupled, either, with a preferential oxidation or a methanation reactor for the final step of the CO removal [1,2].

The cyclic water gas shift (CWGS) reactor concedes as an alternative to the conventional technologies applied for the purification of H_2 by removing CO [5–11]. This process can be carried out in one single reactor without any additional gas post-processing steps. The process is based upon repeated iron oxide reduction/re-oxidation cycles. During the reduction phase of each cycle, CO reduces the iron oxide Fe_3O_4 to an iron compound in its lower oxidation state, FeO_x, according to Eq. (1). During the re-oxidation phase, steam oxidizes FeO_x, and simultaneously, H_2 is produced according to Eq. (2). The gas product from the re-oxidation phase contains a mixture of H_2 and H_2O

* Corresponding author. Tel.: +49 391 6110 318; fax: +49 391 6110 566.
E-mail address: rihko@mpi-magdeburg.mpg.de (L.K. Rihko-Struckmann).

1381-1169/$ – see front matter © 2007 Elsevier B.V. All rights reserved.
doi:10.1016/j.molcata.2007.11.016

and can, therefore, be directly supplied to a PEMFC. The overall reaction for this process is the water gas shift reaction indicated by Eq. (3).

$$\text{Phase I}: \quad (4-3x)CO + Fe_3O_4 \Leftrightarrow (4-3x)CO_2 + 3FeO_x, \quad \Delta_R H < 0 \tag{1}$$

$$\text{Phase II}: \quad (4-3x)H_2O + 3FeO_x \Leftrightarrow (4-3x)H_2 + Fe_3O_4, \quad \Delta_R H > 0 \tag{2}$$

$$\text{Overall}: \quad CO + H_2O \Leftrightarrow CO_2 + H_2, \qquad \Delta_R H < 0 \tag{3}$$

As a whole, this scheme can be seen as a mediated water gas shift reaction, where the CO reducing phase and the H_2 production phase are decoupled in time and use iron oxide material as a mediator that is able to store oxygen. This enables the simple and complete removal of CO from any syngas feed.

The deactivation of the iron oxide material and the decrease of the oxygen exchange capacity over time are the main challenges in the CWGS process. The most critical issue for the overall economic viability of a CWGS process is the ability of the oxygen storage material that is needed to regain its high activity during the repeated reduction/re-oxidation cycles. An important factor for iron-oxide deactivation during the CWGS reaction was found to be the material sintering. This factor can be mitigated by decreasing the operation temperature and by adding a promoter to the iron oxide. We investigated the deactivation of iron oxide material in detail in our earlier work and determined the optimal composition between the iron oxide and the promoter $Ce_{0.5}Zr_{0.5}O_2$ [12]. Another crucial parameter with regards to the CWGS process feasibility is the CO concentration of the H_2 stream produced during the re-oxidation phase. Carbonaceous deposits can be formed on the catalyst surface during the reduction step (Eq. (1)) by means of the Boudouard reaction (4). Such an occurrence leads to the formation of CO by the reaction that takes place during the successive re-oxidation step, as according to Eq. (5):

$$2CO \leftrightarrow C + CO_2 \tag{4}$$

$$C + H_2O \leftrightarrow CO + H_2 \tag{5}$$

The mechanism behind the interaction of CO with the Fe_2O_3–$Ce_{0.5}Zr_{0.5}O_2$ catalyst has not been completely declared.

For the above reasons, the present work was focused on exploring the interaction between the CO and the Fe_2O_3–$Ce_{0.5}Zr_{0.5}O_2$ catalyst by the adsorption investigations under isothermal CO/H_2 exposure and temperature programmed desorption (TPR), isotope exchange investigations and in-situ diffuse-reflectance infrared Fourier transform spectroscopy (DRIFT).

2. Experimental

The preparation of the Fe_2O_3–$Ce_{0.5}Zr_{0.5}O_2$ oxide material used in this study is described in detail in our previous publications [5–7,12]. Therefore, it is only briefly described here. The material was synthesised by urea hydrolysis according to [13,14] whereby the mixed metal salt solution (0.1 M) had been added to a 0.4 M solution of urea (99.0%, Fluka) with a salt to urea solution ratio of 2:1 (v/v). This mixture was mixed at 100 °C for 24 h. After the suspension had been cooled to room temperature, the solid product was separated from the solution. The solid product was washed with ethanol and dried overnight in an oven at 110 °C. Finally, the prepared Fe_2O_3–$Ce_{0.5}Zr_{0.5}O_2$ were calcinated at 800 °C. In our previous studies, the optimal molar ratio between Fe_2O_3 and the promoter $Ce_{0.5}Zr_{0.5}O_2$ was found to be 80/20 [12]. Hence, this oxide ratio was applied to all investigations undertaken in the present paper, and the notification of Fe_2O_3–$Ce_{0.5}Zr_{0.5}O_2$ refers to this material with the above mentioned molar ratio.

The Brunauer–Emmett–Teller (BET) surface area was determined by N_2 adsorption at 77 K using a Quantachrom Instruments NOVA 2000e Analyzer (Quantachrom GmbH, Germany). Prior to the analysis, the samples were outgassed at 250 °C for 4 h to eliminate any volatile adsorbents present on the surface. The surface area was calculated from five adsorption isotherm points obtained for various relative nitrogen pressures (p/p_0) in the range of between 0.05 and 0.3.

The phase analysis of the Fe_2O_3–$Ce_{0.5}Zr_{0.5}O_2$ was performed using X'Pert Pro powder XRD, equipped with an X'celerator detector (Panalytical GmbH, Germany) that uses Cu Kα radiation. The powder patterns were collected in a 2θ scan range from 10° to 80° with a step of 0.017° and a 30-s counting time at each angle. The samples were prepared on the background free silicon single crystal disks.

The adsorption studies under the isothermal exposure of CO/H_2, as well as the temperature programmed desorption (TPD) investigations, were carried out with the BELCAT flow apparatus (Rubotherm GmbH, Germany). The isothermal adsorption study with CO was carried out prior to the classical TPD. The sample (250 mg) was placed in a U-shaped quartz reactor and treated with a flow of He at 400 °C for 2 h, after which the temperature was gradually lowered to the respective operation temperature under a continuous He flow. The isothermal exposure of CO was investigated at temperatures of 60, 150, 250 and 350 °C over a period of 25 min, while, each time, applying a gas mixture of CO/H_2/He with a corresponding molar ratio of 1/2/25. While applying the gas mixture, the composition of the reactor effluent was monitored on-line using the mass spectrometer Agilent 5973 Network Mass Selective Detector. The MS signals with m/z value of 2 (H_2), 14 (H_2O), 28 (CO) and 44 (CO_2) were continuously recorded. The CO peaks were corrected due to the fragmentation of CO_2 ($CO_2 \rightarrow CO + O$) in the spectrometer.

After an adsorption measurement which was carried out isothermally, the sample was subsequently cooled to room temperature under a He flow, and the remaining gaseous CO was swept out of the system. The temperature programmed desorption was, then, carried out by raising the temperature linearly with a rate of 30 °C/min under the a continuous flow of He. During the TPD, the composition of the reactor effluent was monitored on-line using the MS.

$C^{18}O$ isotope exchange experiments were conducted in order to declare the disproportionation (Boudouard reaction) of CO during the CO treatments. A 99.8% isotopically pure $C^{18}O$ was obtained from Aldrich, Germany. During the isotope exchange experiments, the MS signals located at $m/z = 30$ ($C^{18}O$), 46 ($C^{16}O^{18}O$), and 48 ($C^{18}O^{18}O$) were continuously recorded.

Diffuse-reflectance FTIR spectra were collected using a Smart collector and a high temperature Environmental Chamber that was equipped with ZnSe windows (both being from Thermo Electron GmbH, Germany). The FTIR analyzer used in the experiments was a Nicolet 6700 that was equipped with a Ge/KBr beamsplitter and a DLaTGS detector (Thermo Electron GmbH, Germany). The stainless steel gas lines (He, CO, H_2) were connected to the cell. When H_2O was added, the H_2O content was 2.20 vol.% as it was obtained by saturating the He stream with distilled H_2O at 22 °C.

Initially, the catalyst was pre-treated at 450 °C for 60 min under a He flow. The sample was then exposed to a CO/H_2 mixture (5/10 vol.%), and IR spectra were recorded at temperatures of 60, 150, 250 and 350 °C. The presented IR spectra were always recorded against the backgrounds that had been collected immediately prior to the gas exposure at the respective experimental temperature under the continuous flow of He. In order to achieve a good signal-to-noise ratio, a co-addition of 50 scans at the resolution of 4 cm^{-1} were recorded. The changes in the DRIFT spectra were recorded for 5–20 min while exposing the catalyst to a mixture of CO and H_2 in He at the total flow rate of 60 ml/min at each temperature. Subsequently, the samples were purged with He at the operation temperature. The spectra were collected both during the CO/H_2 treatment and during the He purging.

The activity tests for the reduction and re-oxidation of the Fe_2O_3–$Ce_{0.5}Zr_{0.5}O_2$ catalyst were carried out in a packed bed quartz tube reactor (i.d. 10 mm). Typically, 250 mg of the catalyst were packed between the layers of quartz wool. The reactor was placed in an electrical furnace equipped with K-type thermocouples. The temperature of the catalyst bed was measured by thermocouples that had been fixed to the inside and outside of the reactor tube at the position of the catalyst bed.

The reduction phase of one cycle was performed by gas mixtures containing a mixture of CO (20 vol.%) and H_2 (40 vol.%) in He.

Before one re-oxidation phase with steam was started, the H_2 and CO in the lines were removed by purging the system with He for 5 min. Subsequently, the re-oxidation of the reduced catalysts by steam (75 vol.% in He) (phase II of the process cycle) was performed at a flow rate of 120 ml/min. The concentration of the reagents and products was continuously monitored using the Agilent 5973 Network Mass Selective Detector.

3. Results and discussion

3.1. Textural and structural properties of 80 wt.% Fe_2O_3–$Ce_{0.5}Zr_{0.5}O_2$

X-ray diffractograms of Fe_2O_3–$Ce_{0.5}Zr_{0.5}O_2$ are shown in Fig. 1. The samples yielded characteristic reflections that corresponded either to Fe_2O_3 or a cubic structure of a ceria–zirconia solid solution. Furthermore, the XRD analysis of the samples revealed that no binary compounds were formed between the Fe-oxides and Ce-oxides. $FeCeO_3$ compounds with their cerium ions in the Ce^{3+} state were identified neither in the fresh Fe_2O_3–$Ce_{0.5}Zr_{0.5}O_2$ samples, nor in the re-oxidized samples, after several redox cycles. The particle diameter calculated by the standard XRD line broadening method was 30 nm.

Fig. 2 presents a scanning electron microscopy (SEM) image of the used Fe_2O_3–$Ce_{0.5}Zr_{0.5}O_2$ material. The particles detected in the SEM images have the same average size, which had been calculated by the XRD line broadening method. The particles exhibit relatively well-defined spherical-like grains. Some of those grains are overlapping due to the sintering effect that has been discussed in more detail in our previous paper [12]. The BET surface area of the Fe_2O_3–$Ce_{0.5}Zr_{0.5}O_2$ catalyst was 18 m^2/g.

3.2. Activity measurements

Fig. 3 illustrates the average amount of hydrogen produced during the fifth oxidation phase with steam as the oxidant which

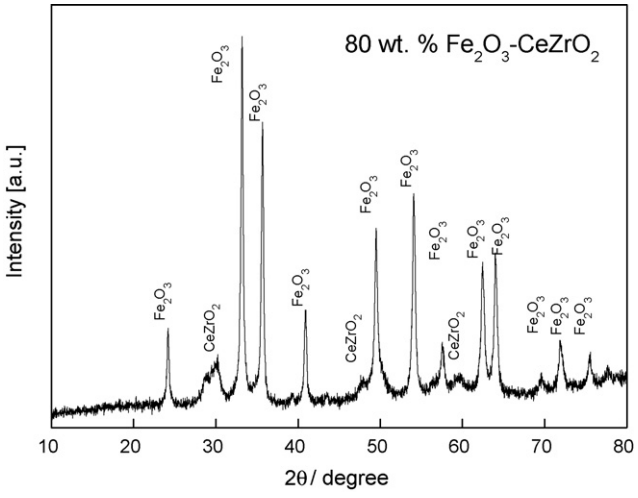

Fig. 1. X-ray diffractograms of Fe_2O_3–$Ce_{0.5}Zr_{0.5}O_2$.

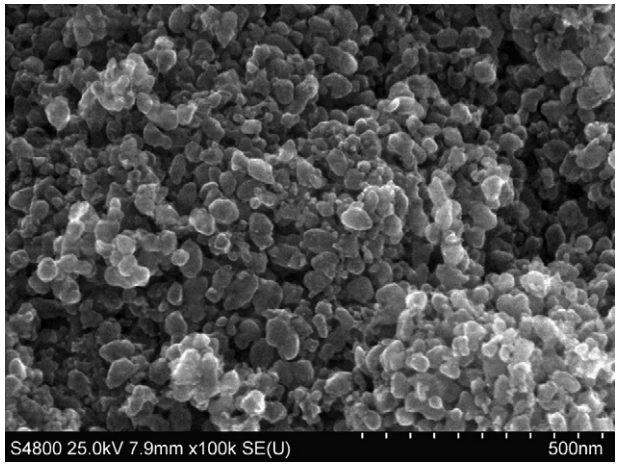

Fig. 2. The SEM images of the Fe_2O_3–$Ce_{0.5}Zr_{0.5}O_2$.

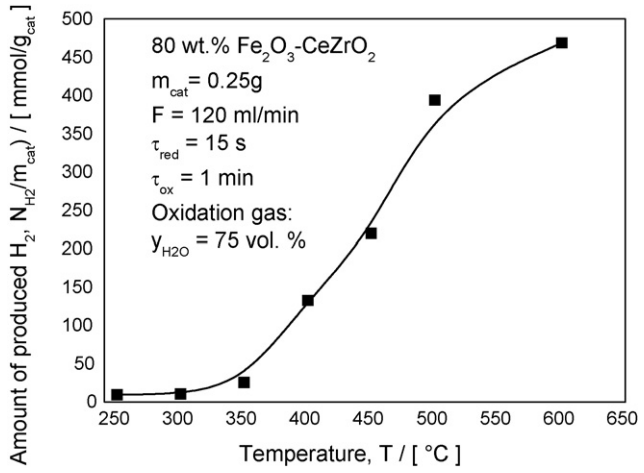

Fig. 3. The amount of the produced H_2 as a function of reaction temperature during the fifth redox cycle with the Fe_2O_3–$Ce_{0.5}Zr_{0.5}O_2$.

is carried out after four complete redox cycles with a reducing gas mixture of 40 vol.% of H_2 and 20 vol.% of CO in He (reduction phase) and steam (oxidation phase). The illustration shows the amount of hydrogen at seven investigated temperatures between 200 and 600 °C. As can be seen in Fig. 3, a temperature increase elevated the amount of produced hydrogen. As discussed above, a re-oxidation reaction using steam (refer to Eq. (2)) does not produce any carbon oxides. However, carbon oxides can be released from the catalyst surface due to the possible steam gasification of chemically adsorbed carbon species on the surface. These species could be formed during the preceding catalyst reduction phase taking place with the presence of CO and H_2. The rate of formation of the CO and CO_2 during one re-oxidation period (about 70 s) is presented in Fig. 4. As can be seen in this figure, the rate of formation of CO and CO_2 decreases with increasing temperature, and at equal re-oxidation times, the rate of CO_2 formation was significantly higher than that of CO. Furthermore, it should be mentioned that at the temperature of 500 °C and above, the rate of CO formation was always below 1 μmol/(min g). The oxygen conversion degree, describing the extent of the reduction, calculated as a ratio of the amount of produced CO_2 and H_2O and the amount of theoretically removable oxygen in Fe_2O_3 and CeO_2 as defined in Eq. (6):

$$X_{O_2} = \frac{N_{H_2O} + 2N_{CO_2}}{3N_{Fe_2O_3} + 0.5N_{CeO_2}} \quad (6)$$

was never higher than 15% in the investigations presented in Fig. 4, even at the highest temperature of 600 °C. From our earlier studies, we could conclude that the formation of the undesired CO in successive re-oxidation phases of the CWGS reaction operated at a temperature higher than 600 °C depends upon the oxygen conversion degree (Eq. (6)) [6]. Therefore, additional experiments were carried out at 600 °C with extremely high oxygen conversion degrees (>80%). In this case, the main carbon oxide product during re-oxidation was CO (not shown here). As concluded in [6], the oxygen conversion should be kept below 60% in order to avoid remarkable carbon deposition on the catalyst surface during the reduction phase, and in such a way to guarantee a low content of CO (<30 ppm) in the hydrogen gas produced during the successive re-oxidation phase.

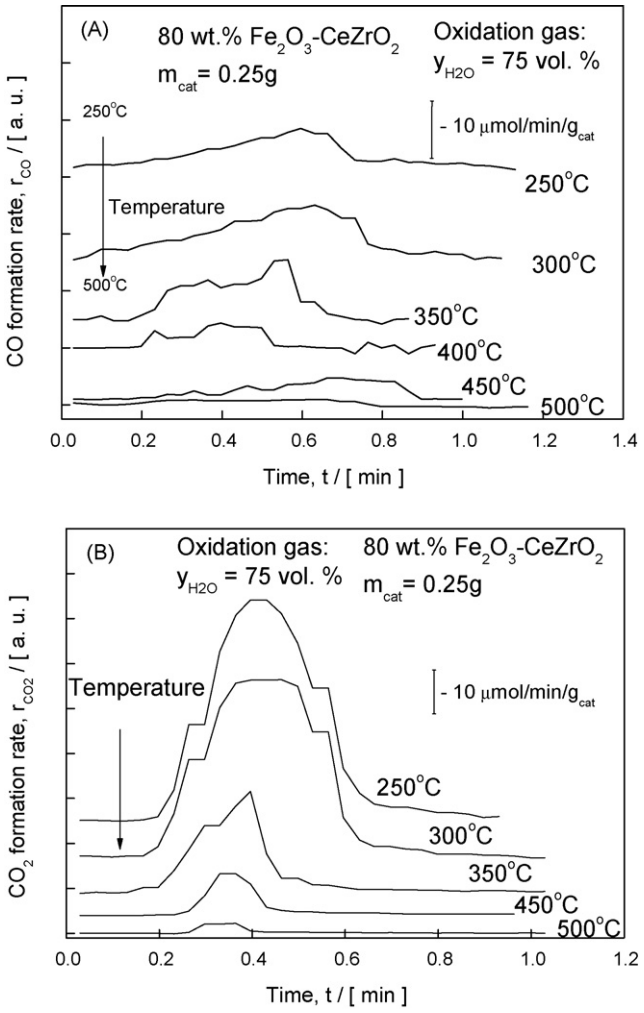

Fig. 4. The rate of the produced (A) carbon monoxide and (B) carbon dioxide as a function of reaction temperature during the re-oxidation period with the Fe_2O_3–$Ce_{0.5}Zr_{0.5}O_2$.

3.3. Isothermal CO/H_2 exposure

The adsorption of CO and H_2 on the Fe_2O_3–$Ce_{0.5}Zr_{0.5}O_2$ catalyst was investigated at temperatures of 60, 150, 250 and 350 °C. Initially, the catalyst was treated with He, and the dynamic change of the reactor outlet concentrations of CO and CO_2 were detected on-line after switching the system to the CO/H_2 exposure. Fig. 5 illustrates the flow rates of CO and the produced CO_2 at the reactor outlet during one adsorption experiment. At the temperature of 60 °C, the material was not likely reacting to a larger extent with the gases as immediately after switching the system to CO/H_2 exposure a constant flow of CO was detected in the reactor outlet, aside from the continuous stream of H_2 (see Fig. 5A). At 150 °C, the formation of CO_2 was also detected as a small, tailing peak appeared after switching the system to the CO/H_2 exposure. The formation of CO_2

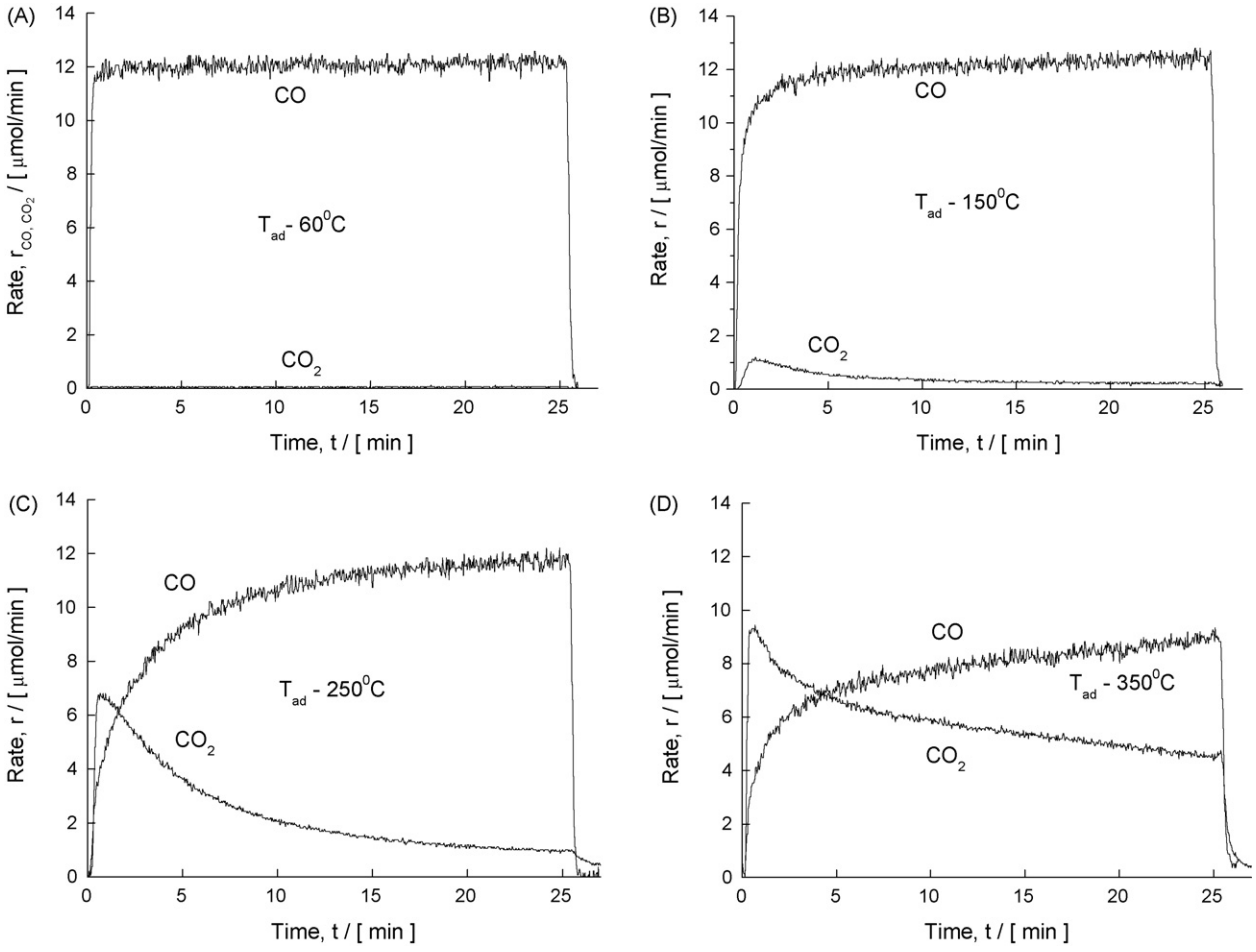

Fig. 5. The observed rate of CO at the reactor outlet during the isothermal exposure of CO and the rate of CO_2 formation in the presence of hydrogen on Fe_2O_3–$Ce_{0.5}Zr_{0.5}O_2$ catalyst at temperatures of: (A) 60 °C; (B) 150 °C; (C) 250 °C; (D) 350 °C.

increased considerably as a function of temperature, as can especially be seen in Fig. 5C and D for the temperatures of 250° and 350 °C. At 350 °C, the rate of CO_2 formation shortly exceeded the flow rate of CO in the outlet.

3.4. Temperature-programmed desorption of CO

After the isothermal CO/H_2 exposure investigations, the samples were cooled to room temperature, and the TPD experiments were subsequently conducted on the same samples. Fig. 6 illustrates the rate of CO release after the isothermal CO/H_2 exposure of the Fe_2O_3–$Ce_{0.5}Zr_{0.5}O_2$ catalyst at temperatures 60, 150, 250 and 350 °C during a TPD experiment. When the CO exposure was carried out at 60 °C, CO_2 was the major product which desorbed within the temperature range of 150–400 °C, having a maximal desorption rate at 240 °C. During the same experiment, a scarcely detectable amount of CO was evolved at 210 °C. With the CO exposure at 150 °C, a distinctly larger amount of CO_2 was released with its desorption maximum being detected at a temperature of 290 °C, whereas a weak CO desorption peak was detected at 300 °C. The most pronounced desorption peaks for CO and CO_2 were observed at the exposure temperature of 250 °C. When the exposure temperature was further increased to 350 or 450 °C, the amount of desorbed CO_2 and CO decreased. After an isothermal exposure at 350 °C, the CO and CO_2 practically desorbed simultaneously. Furthermore, we would like to point out that H_2 consumption during the adsorption experiment was observed only at temperatures higher than 250 °C.

3.5. Isotope exchange investigation

The CO_2 might be formed in the CWGS reaction over two possible routes: (a) the CO might be oxidized by oxygen from the catalyst lattice or (b) the CO disproportionation reaction (Boudouard reaction) might take place on the catalyst under reducing conditions.

In order to enlighten the reactions occurring on the catalyst surface during CO/H_2 exposure, isotope exchange experiments were carried out. The reactions of $C^{18}O$ on the Fe_2O_3–$Ce_{0.5}Zr_{0.5}O_2$ was investigated by the continuous exposure of the catalyst to a 1% $C^{18}O$ gas mixture in He. MS signals at $m/z = 30$ ($C^{18}O$), 46 ($C^{16}O^{18}O$), and 48 ($C^{18}O^{18}O$) were recorded during the experiment. No appreciable amount of $C^{18}O^{18}O$ was detected at temperatures below 350 °C, but it was clearly detected above this temperature. Fig. 7 shows the reactor outlet concentrations of $C^{18}O$, $C^{16}O^{18}O$ and $C^{18}O^{18}O$

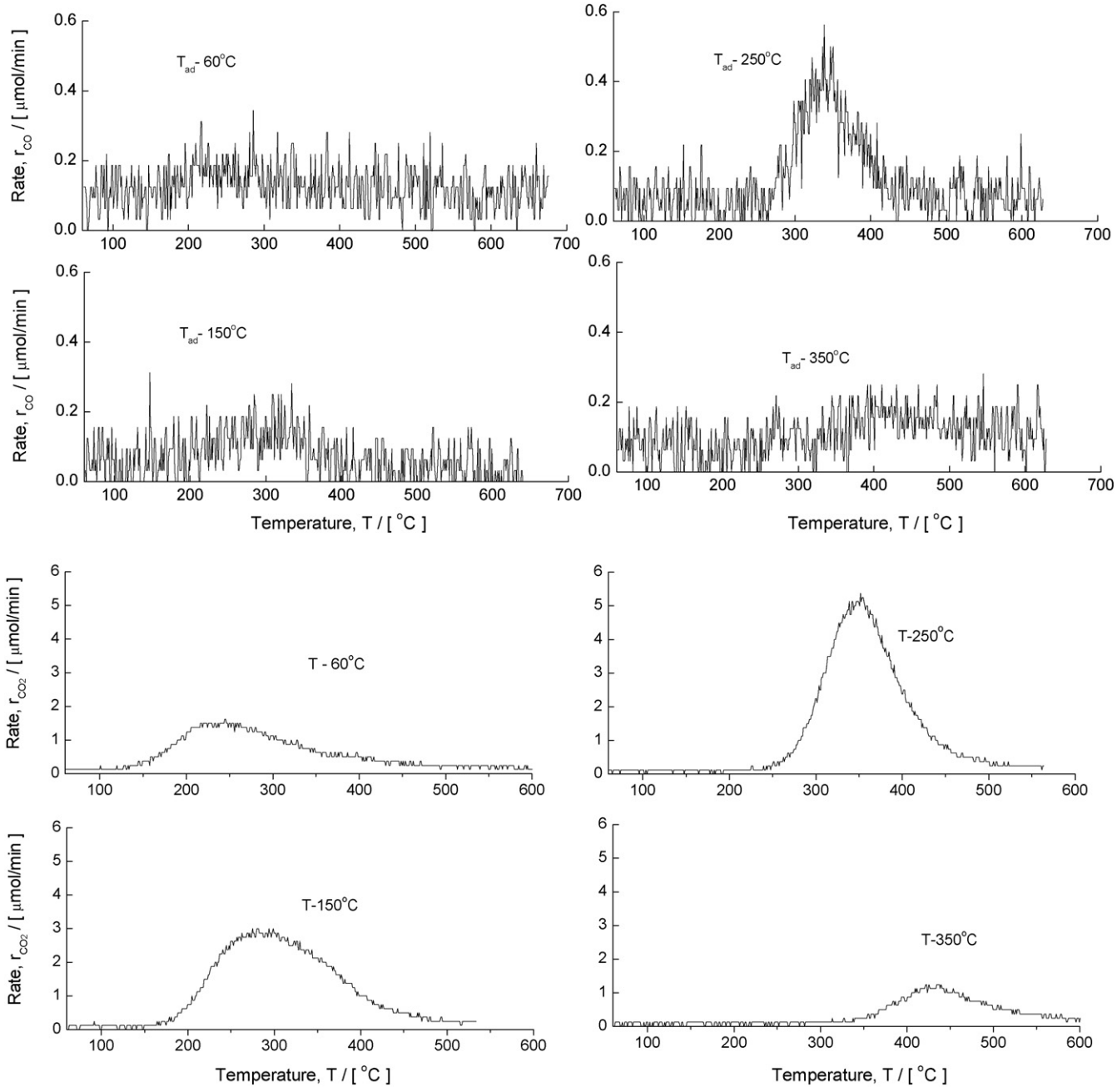

Fig. 6. TPD spectra after isothermal adsorption of CO on Fe_2O_3–$Ce_{0.5}Zr_{0.5}O_2$ catalyst at temperatures 60, 150, 250 and 350 °C: rate of CO desorption (A); rate of CO_2 desorption (B).

during the exposure of the catalyst to $C^{18}O$ at 600 °C. In this figure, we could clearly see that the main product at the initial stage of the experiment was $C^{16}O^{18}O$ and that the consumption of $C^{18}O$ was high. However, during the on-going $C^{18}O$ exposure, the concentration of $C^{16}O^{18}O$ gradually decreased, while the concentration of $C^{18}O^{18}O$, as well as $C^{18}O$, increased continuously. The formation of $C^{16}O^{18}O$ is possible when the catalyst lattice releases oxygen during the reduction phase. The formation of $C^{18}O^{18}O$ can clearly be attributed to the Boudouard reaction (Eq. (4)) that is also responsible for the formation of carbonaceous deposits on the surface. The group of Sun [15] observed a similar phenomenon, where CO_2 was detected during the isothermal adsorption of CO on a reduced Fe–CuMnZrO$_2$ catalyst at 200 °C. It was suggested that carbon monoxide dissociation or disproportionation took place on the catalyst surface. Perrichon [16] investigated the adsorption of $C^{18}O$ on Fe/A1$_2$O$_3$ and Fe/SiO_2 at room temperature by TPD-MS. Two desorption peaks corresponding to the evolution of $C^{18}O$ at 100 °C and of $C^{16}O$ at 400 °C were obtained. These results showed, inevitably, that an exchange of oxygen was occurring through the dissociation of the CO molecule.

Our results confirmed the assumption that CO oxidation is occurring with oxygen coming entirely from the catalyst lattice during CO exposition at temperatures below 350 °C. At tempera-

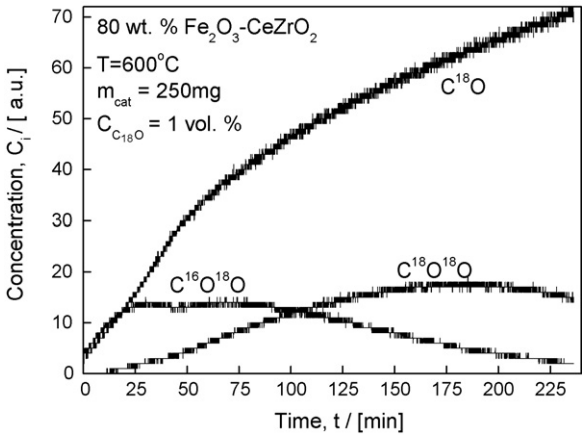

Fig. 7. Reactor outlet concentration of carbon oxides $C^{18}O$, $C^{16}O^{18}O$, and $C^{18}O^{18}O$ during the isotope exchange experiment with Fe_2O_3–$Ce_{0.5}Zr_{0.5}O_2$.

tures above 350 °C, the CO_2 is being produced both by oxidation with the lattice oxygen, as well as by the dissociation of the CO molecule on the catalyst surface.

3.6. Infrared spectra of CO adsorption

Finally, by DRIFT investigations we wanted to clarify in detail, which species are accumulated on the surface during CO and H_2 treatment at various temperatures. Prior to the investigation of the interaction of CO with Fe_2O_3–$Ce_{0.5}Zr_{0.5}O_2$, the untreated sample showed broad peaks attributed to hydroxide and carbonate species at wave numbers of 3400 as well as 1640, 1550, 1320 cm^{-1}. The sample was then treated in He at a temperature of 400 °C for 30 min. The DRIFT analysis which was recorded during the thermal treatment showed that a significant amount of H_2O was removed from the Fe_2O_3–$Ce_{0.5}Zr_{0.5}O_2$ and the carbonate species were converted to CO_2 (not shown here).

When the Fe_2O_3–$Ce_{0.5}Zr_{0.5}O_2$ was treated isothermally with a mixture of CO and H_2 at temperatures of 60, 250 and 350 °C, signals at wave numbers of 1290, 1570, 2060, 2115, 2172, 2337 cm^{-1} were observed (see Fig. 8). The broad peaks at 1290 and 1570 cm^{-1} increased monotonically during the adsorption time (see Fig. 8A). The IR band between 1200 and 1700 cm^{-1} is assumed to be the result of various carbonaceous species adsorbed on the material [17]. At higher temperatures (from 250 to 350 °C), the clearly observable peaks at 2337 and 2361 cm^{-1} could be attributed to the formation of gaseous CO_2. In literature, it has been reported that CO adsorbs on the surface of Au/Fe_2O_3 catalysts and forms carbonate species that, then, undergo hydrogenation to produce carbonate ($–CO_3^{2-}$) or bicarbonate ($–HCO_3^-$) [17,18]. However, bicarbonates are stable only at temperatures below 130 °C [17–19], and they are completely decomposed at temperatures above 200 °C [17–19]. The group of Trovarelli recently reported that the carbonate species are stable on the Ce–Zr mixed oxides during the cyclic oxidation of CO at temperatures higher than 300 °C [20]. Hilaire et al. reported that some carbonate species can block reaction sites during WGS over ceria support catalysts at a temperature of 400 °C [21]. In our investigations, the peaks at 2060, 2115 and

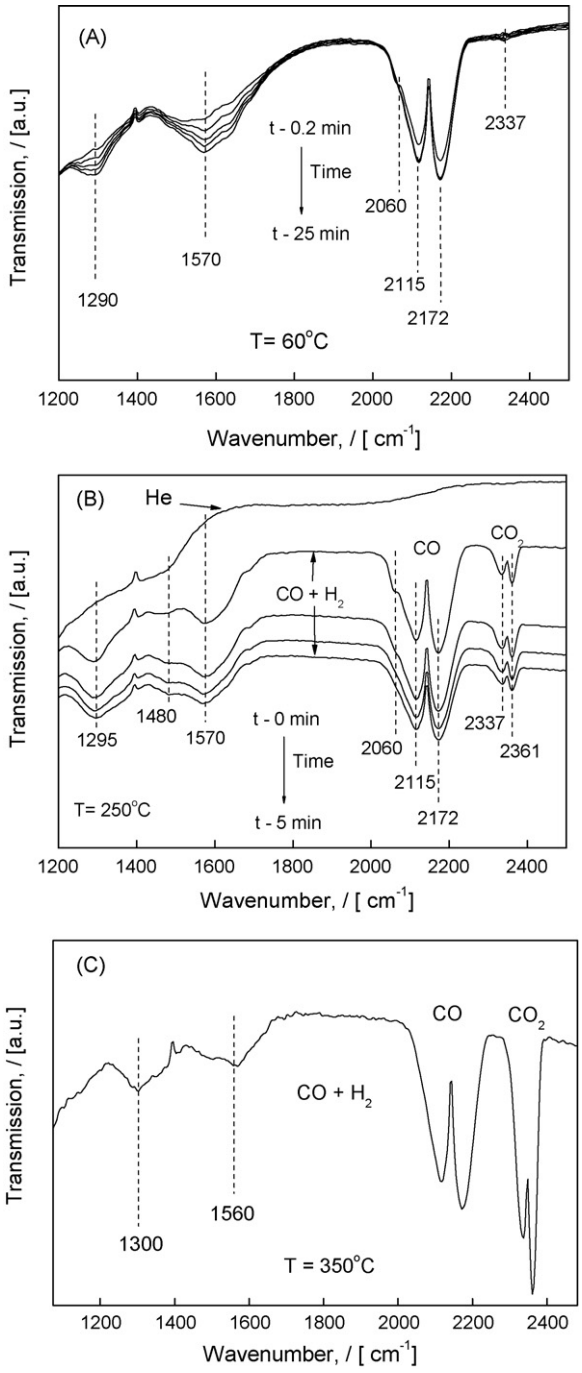

Fig. 8. DRIFT spectra recorded during CO and H_2 exposure on the Fe_2O_3–$Ce_{0.5}Zr_{0.5}O_2$ at temperatures (A) 60 °C; (B) 250 °C; (C) 350 °C.

2172 cm^{-1} can be attributed either to the adsorbed CO, or to the gaseous CO. Those peaks did not change considerably during the exposure. However, during the exposure at the temperature of 350 °C, a peak at 2060 cm^{-1} was not observed (Fig. 8C). The doublet of gaseous CO_2 peaks at 2337 and 2361 cm^{-1} appeared at temperatures of 250 and 350 °C, and they were found to increase with temperature as a result of the very likely catalyst reduction. Therefore, one should remark that the DRIFT data recorded at temperatures higher than 350 °C during the CO and H_2 exposure showed obvious changes in the background,

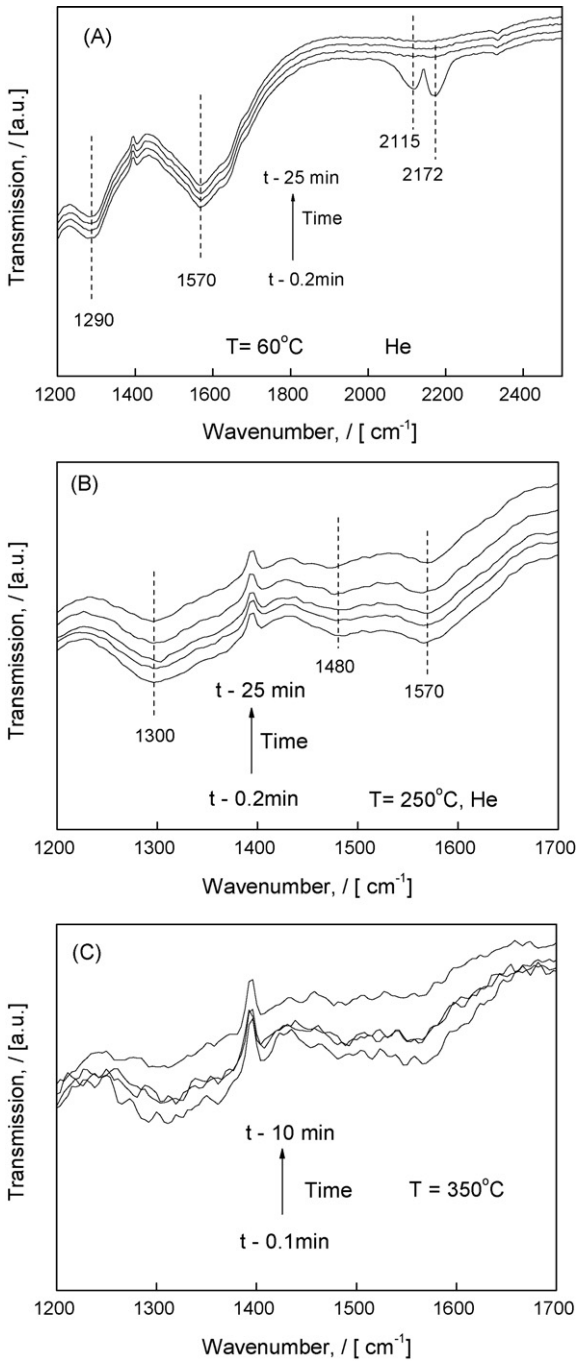

Fig. 9. DRIFT spectra recorded in He atmosphere after the CO and H_2 treatment with Fe_2O_3–$Ce_{0.5}Zr_{0.5}O_2$ at temperatures (A) 60 °C; (B) 250 °C; (C) 350 °C.

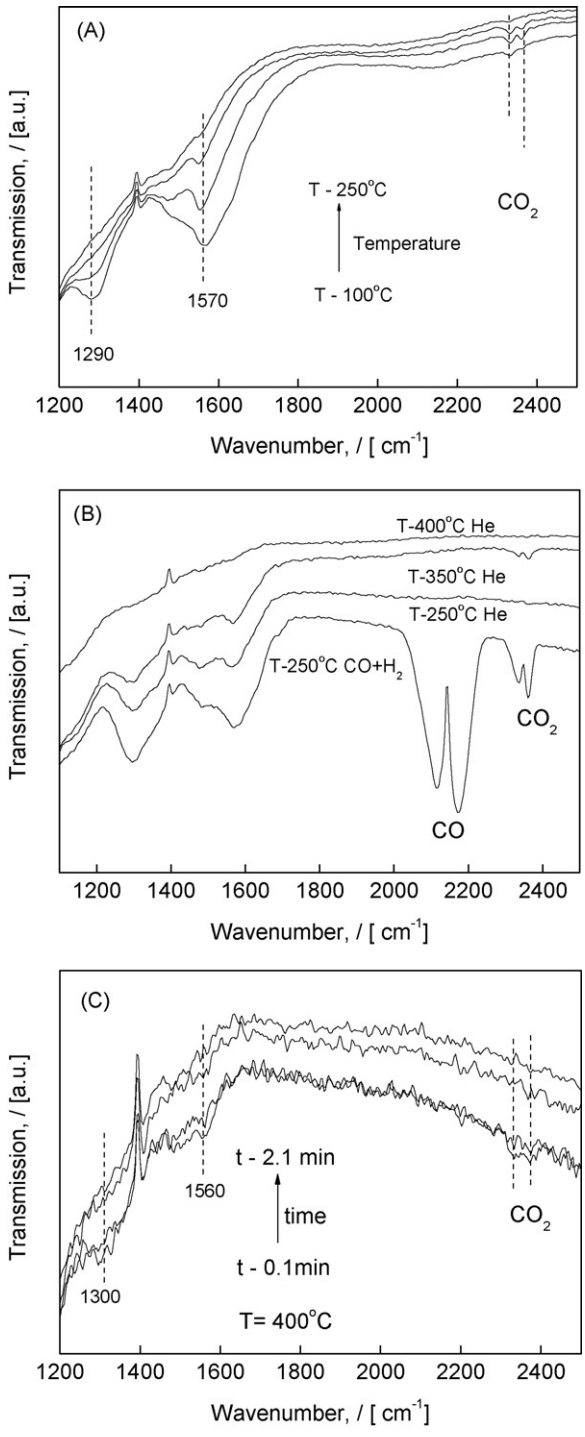

Fig. 10. DRIFT spectra recorded in He atmosphere under increasing temperature after CO/H_2 treatment of Fe_2O_3–$Ce_{0.5}Zr_{0.5}O_2$ at temperatures (A) 60 °C; (B) 250 °C; (C) 350 °C.

due to the reduction of sample which dramatically changed the baseline of the DRIFT spectra.

After CO and H_2 exposures, the treating gas was changed to He, by remaining the investigation temperature constant either at 60 °C (in Fig. 9A), 250 °C (Fig. 9B) or 350 °C (Fig 9C). The peaks attributed to the CO and CO_2 species were found to decrease rapidly, disappearing completely after a few minutes (see Fig. 9). However, the peak assigned to the carbonate-like species (wavenumber 1290–1300 cm^{-1} and 1570 cm^{-1}) remained nearly unchanged during the inert He treatment over 25 min. These adsorbed carbonate species showed high stability at all the investigated temperatures. After the isothermal He treatment, the temperature was subsequently increased. As seen in Fig. 10, under the thermal treatment from 60 to 250 °C (Fig. 10A) the bands attributed to the carbonate-like species disappeared and small bands attributed to CO_2 appeared, most likely, due to the decomposition of the carbonate-like species or due to the reaction with the lattice oxygen. At the temperature of 250 °C, under He treatment the CO and CO_2 bands

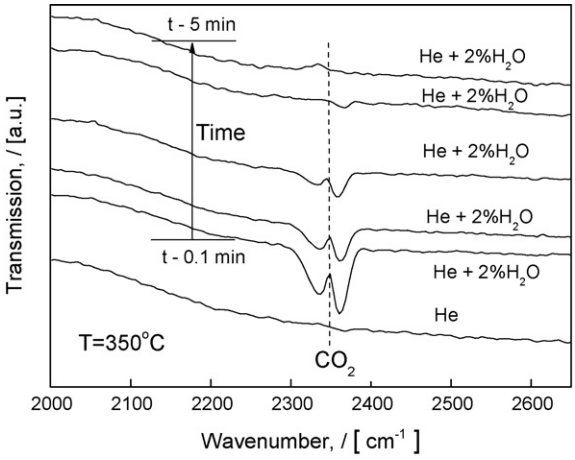

Fig. 11. DRIFT spectra recorded under He and 2.20 vol.% H_2O in He exposure after CO/H_2 treatment of Fe_2O_3–$Ce_{0.5}Zr_{0.5}O_2$ at temperature 350 °C.

disappeared fastly but the carbonate bands in the lower wave numbers after the gradual temperature increase up to 400 °C (Fig. 10B and 10 C). For comparison, the original spectrum under CO and H_2 treatment at 250 °C is illustrated as well in Fig. 10B.

Finally, the influence of an isothermal H_2O/He exposure was investigated, which simulated the conditions during the re-oxidation phase of the CWGS reaction. Initially, the sample was pretreated with CO and H_2 for a period of 15 min. After that, the DRIFT spectra were recorded during the exposure of 2.2 vol.% of H_2O in He (Fig. 11). Two carbon dioxide peaks, having maxima at 2340 and 2370 cm^{-1}, appeared as a result of H_2O and hydroxyl group interconversions with the adsorbed carbonates. The carbonate species were removed from the surface of the sample after a 4 min H_2O exposure.

4. Conclusions

The interaction of CO with the Fe_2O_3–$Ce_{0.5}Zr_{0.5}O_2$ was investigated by TPD, isotope exchange and in situ DRIFT measurements. The data reported here clearly showed that the nature and stability of the carbonate species formed on the Fe_2O_3–$Ce_{0.5}Zr_{0.5}O_2$ depend dramatically upon the reaction conditions.

It was found that the carbonates were the main reaction intermediates under the exposure of H_2 and CO. These carbonates were essentially stable within a He atmosphere in the temperature interval of 60–350 °C. Increasing the sample temperature led to the conversion of the carbonates by oxygen which came from the catalyst lattice. The effect of an H_2O/He mixture showed that carbon oxides were produced during the interconversion of carbonate species on the catalyst surface with steam. However, at a low Fe_2O_3–$Ce_{0.5}Zr_{0.5}O_2$ oxygen conversion degree within the temperature range of 60–500 °C, the main product being produced was carbon dioxide. The amount of produced carbon oxides decreased with elevated temperatures.

The data obtained from isotopic exchange investigations revealed inevitably that the Boudouard reaction is occurring at temperatures higher than 350 °C. The carbonaceous material produced by this reaction on the catalyst surface, then, leads to the formation of CO during successive re-oxidation steps.

Acknowledgments

The authors thank Dr. H. Lorenz for carrying out the XRD investigations. The financial support for this work obtained from the co-operation project between the Fraunhofer Gesellschaft and Max Planck Gesellschaft, *ProBio*, is gratefully acknowledged.

References

[1] C. Song, Catal. Today 77 (2002) 17.
[2] D.L. Trimm, Appl. Catal. A: Gen. 296 (2005) 1.
[3] J.N. Armor, Appl. Catal. A: Gen. 176 (1999) 159.
[4] J. Zhang, Z. Xie, J. Zhang, Y. Tang, C. Song, T. Navessin, Z. Shi, D. Song, H. Wang, D.P. Wilkinson, Z.-S. Liu, S. Holdcroft, J. Power Sources 160 (2006) 872.
[5] V. Galvita, K. Sundmacher, Appl. Catal. A: Gen. 289 (2005) 121.
[6] V. Galvita, T. Schröder, B. Munder, K. Sundmacher, Int. J. Hydrogen Energy, in press.
[7] V. Galvita, K. Sundmacher, Chem. Eng. J., 2007.
[8] V. Hacker, G. Faleschini, H. Fuchs, R. Fankhauser, G. Simader, M. Ghaemi, B. Spreity, K. Friedrich, J. Power Sources 71 (1998) 226.
[9] S. Rossini, U. Cornaro, F. Mizia, A. Malandrino, V. Piccoli, D. Sanfilippo, I. Miracca, Proceedings of the DGMK-Conference on Innovation in the Manufacture and Use of Hydrogen, Dresden, Germany, October 15–17, 2003, pp. 41–47.
[10] K. Otsuka, C. Yamada, T. Kaburagi, S. Takenaka, Int. J. Hydrogen Energy 28 (2003) 335.
[11] M. Thaler, V. Hacker, M. Anilkumar, J. Albering, J.O. Besenhard, H. Schröttner, M. Schmied, Int. J. Hydrogen Energy 31 (2006) 2025.
[12] V. Galvita, T. Hempel, H. Lorenz, L.K. Rihko-Struckmann, K. Sundmacher, Ind. Eng. Chem. Res. 47 (2008) 303–310.
[13] S. Pengpanich, V. Meeyoo, T. Rirksomboon, K. Bunyakiat, Appl. Catal. A: Gen. 234 (2002) 221.
[14] J. Subrt, J. Bohacek, V. Stengl, T. Grygar, P. Bezdicka, Mater. Res. Bull. 34 (1999) 905.
[15] R. Xu, Z.-Y. Ma, V. Yang, W. Wei, W.-H. Li, Y.-H. Sun, J. Mol. Catal. A: Chem. 218 (2004) 133.
[16] V. Perrichon, React. Kinet. Catal. Lett. 21 (1982) 517.
[17] T. Tabakova, F. Boccuzzi, M. Manzoli, D. Andreeva, Appl. Catal. A 252 (2003) 385.
[18] F. Boccuzzi, A. Chiorino, M. Manzoli, D. Andreeva, T. Tabakova, J. Catal. 188 (1999) 176.
[19] B. Aeijelts Averink Silberova, G. Mul, M. Makkee, J.A. Moulijn, J. Catal. 243 (2006) 171–182.
[20] M. Boaro, F. Giordano, S. Recchia, V. Dal Santo, M. Giona, A. Trovarelli, Appl. Catal. B: Environ. 52 (2004) 225.
[21] S. Hilaire, X. Wang, T. Luo, R.J. Gorte, J. Wagner, Appl. Catal. A: Gen. 215 (2001) 271.